Chinese Chemical Letters 36 (2025) 110763

Contents lists available at ScienceDirect

Chinese Chemical Letters

journal homepage: www.elsevier.com/locate/cclet

Facile synthesis of all-carbon fluorinated backbone polymers containing sulfide linkage as proton exchange membranes for fuel cells

Yuetong Gao, Tong Mu, Xinyue Hu, Yang Pang, Chengji Zhao*

Key Laboratory of High Performance Plastics, Ministry of Education, College of Chemistry, Jilin University, Changchun 130012, China

ARTICLE INFO

Article history:
Received 25 October 2024
Revised 11 December 2024
Accepted 12 December 2024
Available online 13 December 2024

Keywords:
All-carbon backbone
Proton exchange membrane
Fuel cells
Facile synthesis
Low hydrogen permeability

ABSTRACT

Aryl-ether bonds are facile to attack by oxidizing radicals, thus stimulating the exploitation of ether-free polymers as proton exchange membranes (PEMs) for the long-lasting operation of fuel cells. In this study, a novel class of PEMs derived from all-carbon fluorinated backbone polymers containing sulfide-linked alkyl sulfonic acid side chains have been developed through a straightforward and effective synthetic procedure. The sulfide-linked alkyl sulfonate groups were tethered to the poly(triphenylene pentafluorophenyl) backbone through a quantified and site-specific *para*-fluoro-thiol click reaction. Owing to the existence of obvious phase separation morphology between hydrophobic main chain and hydrophilic sulfonate groups in the side chains, resulting PEMs demonstrated favorable proton conductivity of 142.5 mS/cm at 80 °C, while maintaining excellent dimensional stability with an in-plane swelling ratio of <17% as well as a through-plane swelling ratio of <25%. They also exhibit elevated thermal decomposition temperatures ($T_{d5\%}$ exceeding 300 °C) alongside high tensile strength (>50 MPa). Furthermore, the ether-free full-carbon fluorinated main chain and the -S- group in the side chain, which serves as an effective free-radical scavenger, providing good chemical stability during Fenton's test. The PEMs achieved a maximum power density of 407 mW/cm^2 in a single H_2/air fuel cell, and an open-circuit voltage decline rate of 0.275 mV/h in a durability test at 30% RH and 80 °C. Concurrently, the hydrogen crossover current density is only 1/3 of that of Nafion 212. These findings reveal that the resulted PEMs display considerable antioxidative properties along with commendable performance, with prospective applications in proton exchange membrane fuel cells.

The over-exploitation and excessive use of fossil fuels have resulted in a critical situation concerning energy depletion and environmental pollution for humanity. To realize the carbon neutrality goal, the exploitation of economic and sustainable green energy has become an important proposition for modern society [1,2]. Therefore, scientists are energetically developing cost-effective and highly efficient electrochemical devices for the large-scale renewable energy conversion and storage applications [3–5], such as fuel cells. Proton exchange membrane (PEM) is an essential component of proton exchange membrane fuel cells (PEMFCs). It plays a vital role in the rapid conduction of charged ions and the isolation of anode and cathode materials. Consequently, the development of inexpensive, highly effective, durable, and selective membranes is a pressing necessity to facilitate the large-scale deployment of green energy systems [6–8].

Nafion® is currently the benchmark PEM for applications in PEMFC system, attributing to its high proton conductivity, favorable mechanical and electrochemical properties. Nevertheless, several significant challenges, including high production cost, high gas permeability, have significantly impeded the further advancement of Nafion®. In the past decades, researchers have developed many kinds of sulfonated aromatic polymers for use in PEMs. These polymers exhibit several advantages, including low gas permeation and low cost. However, a notable disadvantage is the prevalence of instable linkages within the polymer main chain, like aryl ether bonds, which render them less stable against oxidation [9–15]. For instance, Nguyen *et al.* prepared a series of sulfonated poly(aryl ether ketone) (SPAEK) membranes, which demonstrated a residual weight of only 90.3% following an hour of submersion in Fenton's reagent at 60 °C. This value is inferior to that of the commercial Nafion 115 membrane (99.9%) [10]. Liu *et al.* prepared a semi-interpenetrating polymer network (semi-IPN) PEM based on SPEEK, with a residual mass of 94.1% after 1 h in Fenton's reagent at 60 °C, which is smaller than that of Nafion 117 (97.9%) [16]. Li *et al.* also

* Corresponding author.
E-mail address: zhaochengji@jlu.edu.cn (C. Zhao).

https://doi.org/10.1016/j.cclet.2024.110763
1001-8417/

prepared sulfonated poly(ether ketone)-poly(ether ketone) copolymers with controlled degree of sulfonation, which broke after only 125 min of immersion in Fenton's reagent (3% H_2O_2 + 2 ppm $FeSO_4$) at 80 °C [17]. This appearance might be ascribed to backbone scission due to the breakage of C–O bonds in the oxidizing environment of strong sulfuric acid. The findings demonstrate that the existence of aryl-ether bonds in the main chain significantly reduce the antioxidant stability of the polymer.

Recently, all-carbon backbone aromatic polymers have attracted considerable attention as alternative materials to PEMs [18]. The presence of rigid phenyl moieties in the main chain endows them with excellent thermostability and mechanical strength, while the lack of heteroatoms mitigates the oxidative deterioration associated with free radical attack. Therefore, a series of ether-free PEMs based on all-carbon backbone aromatic polymers have been developed *via* the Friedel-Crafts reaction [19,20]. These PEMs exhibit superior proton conductivity and moderate antioxidant capacity in comparison to Nafion® membranes. Xu *et al*. prepared novel PEMs based on polymers of intrinsic microporosity (PIMs) through the ultra-strong acid-catalyzed Friedel-Crafts reaction. The rigid and contorted backbone of the sulfonated polymers impedes conformational alterations and disrupts the effective polymer chains stacking, thereby facilitating the establishment of micropores that serve as optimal transport channels for rapid proton and cation transport [21]. Lin *et al*. prepared all-carbon backbone polymers *via* the copolymerization of 7–bromo-1,1,1-trifluoroheptan-2-one, and then tethered flexible alkyl sulfonic acid groups as the proton carriers to the polymer main-chain [22]. The resulted membranes exhibited high proton conductivity of 311 mS/cm at 80 °C. Furthermore, the assembled H_2/O_2 fuel cell exhibited excellent performance with a peak power density of 2.62 W/cm^2. However, the grafted side chains comprising sulfonate groups are vulnerable to fracture due to oxidizing radical attack, which results in a reduction in membrane's conductivity and durability.

To address the vulnerability of sulfonated all-carbon backbone polymers to oxidizing environment, and then improve the durability of PEMFCs, varieties of strategies have been proposed to strengthen the PEM's stability in oxidation environment. Currently, these strategies primarily focus on the introduction of free radical scavengers (FRSs) into the matrix of the membrane [23–27]. However, the mobile FRSs can easily leach out of the membrane under the operation condition of PEMFCs. Therefore, immobilization of FRSs onto the polymer chains is more effective than the physical doping of FRS due to the presence of chemical bonding [28,29], which can mitigate the loss problem of FRSs and its detrimental effect on the proton conductivity.

In this study, a series of sulfide-linked sulfonated poly(triphenylene pentafluorophenyl) polymers were synthesized by the superacid-catalyzed Friedel-Crafts polycondensation reaction, followed by grafting alkyl sulfonate groups to the polymer main chain through a quantified and site-specific *para*-fluoro-thiol click reaction, which is displayed in Fig. 1a. The combination of the fluorinated hydrophobic rigid main chain and the flexible long alkyl sulfonate side chains therein facilitate the formation of more developed and homogeneous hydrophobic and hydrophilic microphase separation morphology. The presence of rigid triphenylene in the main chain also facilitates the enhancement of gas barrier ability, which is favorable for its long-term application in fuel cells. The incorporation of two fluorine-containing monomers, octafluoroacetophenone and pentafluorobenzaldehyde, can enhance the polarity disparity between the hydrophilic and hydrophobic phases of the membranes, facilitating the development of an optimal microphase separation structure within the membranes. Specially, the incorporation of -S- linkage with a free radical scavenging function enhances the polymer's resistance to free radical attack. Photos of the two prepared PEMs are shown in Fig. 1b, and both membranes possess good integrity and transparency. Furthermore, the structure and physiochemical behaviors of the resulting PEMs were investigated in detail, including microphase structure, proton conductivity, dimensional stability, mechanical strength, thermostability and oxidative stability. Finally, the prepared PEMs were subjected to the performance and durability evaluation in H_2/air PEMFCs and compared with those of commercial Nafion 212 membrane.

The superacid-catalyzed Friedel-Crafts polycondensation reaction was utilized to synthesize the PTPFB and PTOFP precursors from *p*-terphenyl with pentafluoro benzaldehyde and octafluoroacetophenone, respectively [30,31]. Subsequently, the sulfonated all-carbon aromatic polymers with a sulfide linkage were obtained by grafting sodium 3-mercapto-1-propanesulfonate (SMPS) onto the side chain through an efficient and site-specific *para*-fluoro-thiol click reaction. Verification of the successful polymerization and grafting reactions was carried out using ^{1}H and ^{19}F NMR spectra as depicted in Fig. S1 (Supporting information). The characteristic peaks at 7.0–8.0 ppm in the ^{1}H NMR spectra ($CDCl_3$) of the precursors PTPFB and PTOFP were assigned to protons on the benzene ring, while the peak appearing at 6 ppm was assigned to protons on the tertiary carbons of the PTPFB main chain. After grafting of SMPS through a *para*-fluoro-thiol click reaction, the obtained polymers became insoluble in chloroform due to a change in polarity. Accordingly, the chemical structures of PTOFP-SMPS and PTPFB-SMPS polymers were characterized using NMR with deuterated DMSO. Three new characteristic peaks appeared between 1.5 ppm and 3.5 ppm, which can be identified as the methylene groups on the SMPS. Furthermore, the complete disappearance of *para*-fluorine signals on the benzene ring at around −155 ppm was observed in the ^{19}F NMR spectra of PTOFP and PTPFB after the grafting reaction. This indicates that the *para*-fluorine on the benzene ring of PTOFP and PTPFB were entirely replaced by SMPS following the grafting reaction, confirming that the grafting ratio of PTOFP-SMPS and PTPFB-SMPS was 100%. Additionally, the grafting process caused a downward shift in the chemical shift of *para*-fluorine from −160 ppm to −134 ppm, which can be attributed to the change in electronegativity. The NMR results confirm the successful preparation of both PTOFP and PTPFB polymers, as well as the complete conduction of the *para*-fluoro-thiol click reaction.

The molecular weight of polymers significantly affects their mechanical performances [32]. GPC tests were conducted to characterize the molecular weight of the precursors PTOFP and PTPFB, because both PTOFP-SMPS and PTPFB-SMPS were insoluble in DMF. As shown in Table S1 (Supporting information), both polymers exhibited a number average molecular weight (M_n) greater than 35 kDa and a weight average molecular weight (M_w) greater than 90 kDa. This confirms that the polymers prepared by the superacid-catalyzed Friedel-Crafts polycondensation reaction have high molecular weight, which contribute to favorable mechanical properties for application in fuel cells.

Ion exchange capacity (IEC) represents a critical parameter for assessing the hydration properties and determining the proton conductivity of PEMs. The theoretical and experimental values of IEC were determined through a theoretical approach based on polymer structure and an experimental approach based on acid-base titration, respectively. As indicated in Table S3 (Supporting information), the experimental IEC values were approximate to theoretical ones. Due to the higher content of sulfonate groups in the polymer, PTPFB-MPSA membrane exhibits a higher IEC of 1.68 mmol/g than that of PTOFP-MPSA membrane. Furthermore, the measured values of WU and SR for PTOFP-MPSA and PTPFB-MPSA are illustrated in Fig. S2 and Table S3 (Supporting information). The water uptake behaviors of both membranes exhibited two principal tendencies. Primarily, all membranes' water uptake raised in accordance with the increase in temperature. This is as-

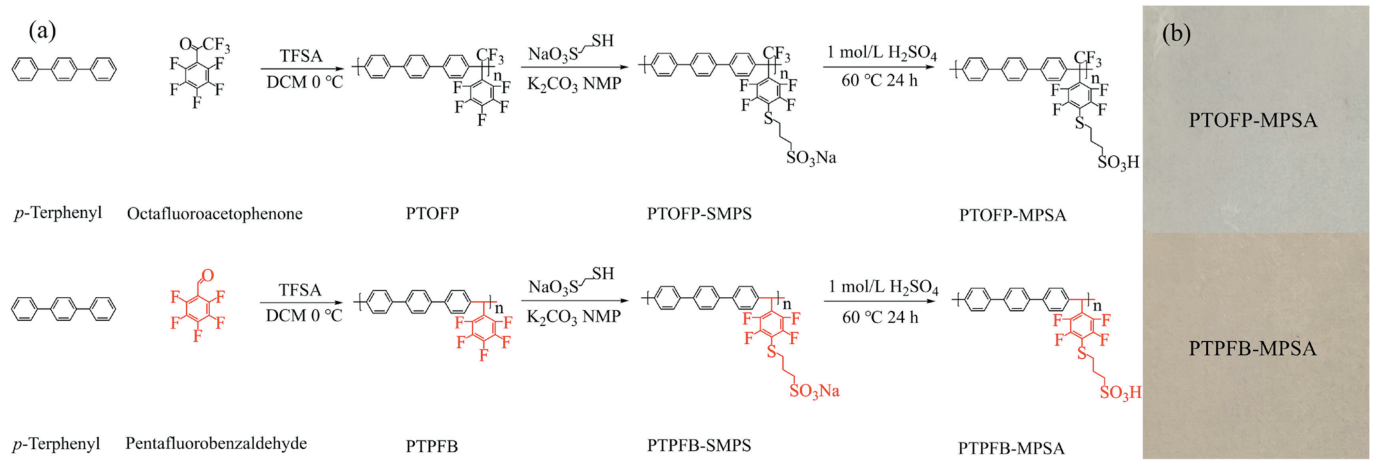

Fig. 1. (a) Synthesis route of PTOFP-MPSA and PTPFB-MPSA. (b) The photos of PTOFP-MPSA and PTPFB-MPSA.

cribed to the result that higher temperatures enhance the free volume within the polymer and its interaction with water [33]. Secondly, high content of sulfonate groups on the polymer enhances the hydrophilicity of PEMs, thereby enabling the membranes to absorb a greater quantity of water. Consequently, at 80 °C, the water uptake of the PTPFB-MPSA membrane was found to be 51.6%, in comparison to 42.1% for the PTOFP-MPSA membrane. Notably, the increase in water uptake from 30 °C to 80 °C is minimal (under 10%), as a result of the rigidity and higher molecular weight of the PTOFP-MPSA backbone [34]. As illustrated in Table S3, the in-plane swelling ratios of PTOFP-MPSA and PTPFB-MPSA membranes were <14% at 30 °C and <20% at 80 °C, while the through-plane swelling ratios were <18% at 30 °C and <25% at 80 °C, both of which were less than those of Nafion 212 membrane. This observation is due to the stiff and hydrophobic aromatic backbones, which confer good dimensional stability [35]. As expected, PTPFB-MPSA membrane showed higher WU and SR values, which could be explained by the absence of the hydrophobic -CF_3 group on the main chain of PTPFB-MPSA. In conclusion, both PTOFP-MPSA and PTPFB-MPSA membranes demonstrate excellent dimensional stability and possess significant advantages in PEMFC application.

During the manufacturing of a membrane electrode assembly (MEA), pressure was usually exerted on PEMs under a repeated dry-wet changing condition of fuel cells, which can cause mechanical degradation over time. Therefore, it is critical that PEMs have good mechanical strength to assure their long-term application in fuel cells [36]. The stress-strain curves of PTOFP-MPSA and PTPFB-MPSA in the dry state measured using an electronic universal testing machine are displayed in Fig. S3a (Supporting information). As presented in Table S2 (Supporting information), both PTOFP-MPSA and PTPFB-MPSA membranes have a tensile strength greater than 50 MPa, indicating that they satisfy the requisite mechanical strength criteria for fuel cell assembly and manipulation. Meanwhile, PTOFP-MPSA's elongation at break is much higher than that of PTPFB-MPSA, attributed to the higher molecular weight of PTOFP-MPSA. The molecular chains are more tightly entangled with each other for PTOFP-MPSA, resulting in an increased elongation at break [37].

PEMs are required to possess excellent thermal stability to avoid thermal degradation during long-lasting operation of fuel cells [38]. Thermogravimetric analysis (TGA) was used to evaluate the thermostability of PTOFP-MPSA and PTPFB-MPSA, with the findings illustrated in Fig. S3b (Supporting information). The thermal degradation process of both PEMs was consistent, with the first decomposition of pendant sulfonate groups in the side chains between 250 °C and 400 °C, with the subsequent decomposition of

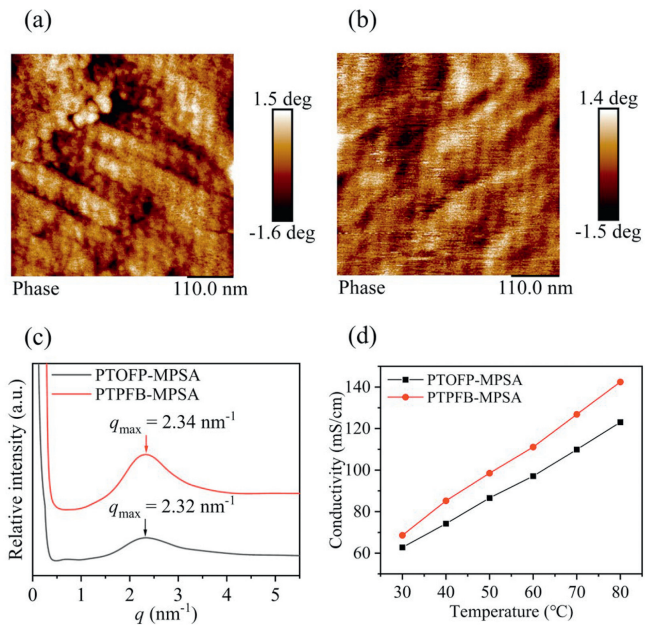

Fig. 2. AFM phase diagrams of (a) PTOFP-MPSA and (b) PTPFB-MPSA, SAXS intensity profiles of (c) PTOFP-MPSA and PTPFB-MPSA and (d) proton conductivity plot *versus* temperature of PTOFP-MPSA and PTPFB-MPSA.

the polymer main chain proceeding between 400 °C and 600 °C. Table S2 shows that the temperature for 5% weight loss ($T_{d5\%}$) exceeded 300 °C for both PEMs. This observation confirms that both PEMs exhibit excellent thermal stability, rendering them appropriate for application in fuel cells.

The microstructures of PTOFP-MPSA and PTPFB-MPSA were analyzed using AFM phase diagrams. The darker regions represent hydrophilic ionic regions resulting from the existence of pendant sulfonate groups in the side chains, while the brighter regions represent hydrophobic regions derived from all-carbon fluorinated aromatic backbone. As illustrated in Figs. 2a and b, both PTOFP-MPSA and PTPFB-MPSA membranes exhibit obvious phase-separated microstructures, resulting from the polarity difference between the hydrophilic sulfonate group in the side chains and the hydrophobic main chain of the fluorophenyl group [39]. SAXS can quantitatively reflect the domain spacing of the membranes and investigate the phase separation behavior of PTOFP-MPSA and PTPFB-MPSA membranes. As detailed in Fig. 2c and Table S3, the

SAXS profiles of both membranes showed a well-defined scattering peak at a low scattering vector (q), indicative of the formation of highly-developed phase-separated structures within the membranes. The domain spacing (d) of both membranes determined through the Bragg equation ($d=2\pi/q$) are approximately 2.70 nm. In conclusion, the phase-separated morphology facilitates the development of homogeneous and continuously distributed proton transport channels within the membranes, thereby accelerating proton conduction through these channels.

The proton conductivities of PTOFP-MPSA, PTPFB-MPSA as a function of temperature in the region from 30 °C to 80 °C are illustrated in Fig. 2d and Table S3. It was observed that the proton conductivity of all PEMs exhibited an enhancement with the rising temperature. For the PTPFB-MPSA membrane, the proton conductivity significantly increased to 142.4 mS/cm, as the temperature rose to 80 °C. The value was superior to that of PTOFP-MPSA (123.1 mS/cm), attributed to the augmentation of WU and IEC of PTPFB-MPSA. The enhancement of WU leads to an enhancement in the proportion of hydrophilic regions within the membrane, which facilitates rapid proton transport, as the transfer of H^+ within the membrane requires hydrated hydrogen ions to act as a transport medium. Additionally, the augmented IEC facilitates a greater quantity of sites for transporting H^+, thereby enhancing the rate of proton conduction. The activation energy of two PEMs for proton conduction was calculated employing the Arrhenius equation. The results are detailed in Fig. S4 (Supporting information). All membranes exhibit low proton conduction activation energy. This is explained by the formation of continuous ionic clusters within the membranes, which has been confirmed by AFM and SAXS observations [40]. Furthermore, it is evident that PTOFP-MPSA exhibits a lower proton transfer activation energy compared to PTPFB-MPSA, which can be explained by the existence of an additional hydrophobic group (-CF_3) on the backbone. This group strengthens the structure of microphase separation and promotes the development of the H^+ transfer channels, thus reducing the activation energy of H^+ transfer. However, both PEMs prepared in this study contain aryl structures. To further investigate the effect of aryl groups on proton transfer, the proton transfer activation energies (E_a) of the two PEMs were calculated using the Arrhenius equation and compared with those of PEMs without aryl groups in the literature. The results presented in Table S4 (Supporting information) indicate that both the water absorption and E_a of PEMs with aryl structures in the main chain are lower than those of PEMs without aryl groups in the main chain. This suggests that the introduction of aryl groups may facilitate the transfer of protons. This effect can be attributed to the generally more rigid and hydrophobic nature of aryl structures compared to the aliphatic structure lacking aryl groups [41]. Consequently, this reinforces the polar difference between the hydrophilic and hydrophobic domains within the membrane, thus promoting the formation of phase-separated structures.

Over extended operation of a fuel cell, the permeation of hydrogen through the PEM to the cathode results in an incomplete oxygen reduction reaction (ORR) at the cathode. This phenomenon gives rise to the generation of highly reactive free radicals ($H^•$, $OH^•$, $OOH^•$). These radicals attack the polymer's main chain and induce its chemical degradation, causing a deterioration in the mechanical strength of PEMs [38,42]. Besides, free radicals can attack the acidic pendant groups of the polymer, thereby impairing proton conduction [43]. Therefore, the ability of PEMs to withstand oxidative degradation is a pivotal parameter for evaluating the durability of fuel cells. Fenton's reagent is commonly employed to simulate accelerated degradation conditions of PEMs. In this study, a Fenton's reagent concentration of 3% H_2O_2, 2 ppm Fe^{2+} was utilized. The residual weight of PTOFP-MPSA and PTPFB-MPSA in the dry state was recorded following the Fenton's reagent treatment. As shown in Table S2, the residual weight of both membranes exceeded 98% after two hours of immersion, indicating that both membranes exhibit good oxidation resistance. Meanwhile, the higher residual weight of PTOFP-MPSA compared to PTPFB-MPSA after 2 h of immersion can be ascribed to the -CF_3 group on the backbone of PTOFP-MPSA, which is beneficial to enhancing its resistance to free radicals. The -C-F- bond possesses high bond energy, and the fluorine atom has a large radius, facilitating the formation of a protective layer around the polymer backbone, thus shielding it from free radical attack [44]. As the number of fluorine atoms increases, the polymer backbone is more effectively shielded from free radical attack.

To monitor the structural changes of PTOFP-MPSA and PTPFB-MPSA during the Fenton's test, their ^{1}H NMR and FT-IR spectra before and after Fenton's reagent treatment were analyzed. Take Fig. 3a as an example, PTOFP-MPSA exhibit a gradual shift to the high field for the two proton signal peaks (H5, H6) corresponding to the -CH_2- groups distant from -S- group with an increase in immersion time. Additionally, the peak (H4) corresponding to the -CH_2- group adjacent to the -S- group splits into two peaks, with one shifting to a higher field (H4") and the other to a lower field (H4′). The side chains of PTOFP-MPSA underwent a transformation from -S- group to the -SO- group and subsequently to the -SO_2- group after being attacked by free radicals. Following the transformation of the -S- group to the -SO- group, the proton peak of H4 shifts to a lower field, while the proton peaks of H5 and H6 shift to a higher field. Conversely, when the -SO- group is transformed to -SO_2- group, the proton peak of H4 shifts to a higher field, while the proton peaks of H5 and H6 continue to shift to a higher field. This indicates that some of the -S- groups were converted to -SO- group, while others were converted to the -SO_2- group in two steps following a 2 h immersion of PTOFP-MPSA in the Fenton's reagent. The aforementioned characterization of proton peak migration is also evident in Fig. 3b. The results suggest the -S- linkage acts as a free radical scavenger in the Fenton's reagent test. Furthermore, as illustrated in Fig. 3b, three proton peaks corresponding to the -CH_2- groups associated with -S- linkage (H5, H6, H7 in Fig. 3b) were still observed after 1 h of immersion, which completely disappeared in Fig. 3a. This discrepancy may be attributed to the additional -CF_3 group on the main chain of PTOFP-MPSA, which provides enhanced protection for the main chain, thereby facilitating free radical attack upon the -S- linkage in the side chain, resulting in the complete transformation within the aforementioned interval. The reduction in the integrated area of the proton peak corresponding to the hydrogen on the tertiary carbon of the backbone of PTPFB-MPSA (H4 in Fig. 3b) indicates that the lack of -CF_3 protection of the main chain of PTPFB-MPSA results in a certain extent of degradation. As illustrated in Figs. 3c and d, there was no discernible alteration in the characteristic peak intensity of the -SO_3H group at 1030 cm^{-1} for PTOFP-MPSA and PTPFB-MPSA during evaluation with Fenton's reagent. Furthermore, the characteristic peak intensity of the -SO_2- group at 1179 cm^{-1} for PTOFP-MPSA and PTPFB-MPSA was observed to increase, suggesting that -SO- group was gradually converted to -SO_2- group with the increase of immersion time. Consequently, we put forth a possible mechanism through which the -S- group could serve as a free radical scavenger, as illustrated in Fig. 3e. This mechanism was subsequently validated in some published reports [45,46].

In conclusion, the -S- linkage played the role of a free radical scavenger in the free radical-rich environment of Fenton's reagent, which significantly enhanced the antioxidant stability of PTOFP-MPSA and PTPFB-MPSA membranes. Meanwhile, the additional -CF_3 group in PTOFP-MPSA provided superior protection to the main chain, which explains the higher residual weight of PTOFP-MPSA after Fenton's reagent testing.

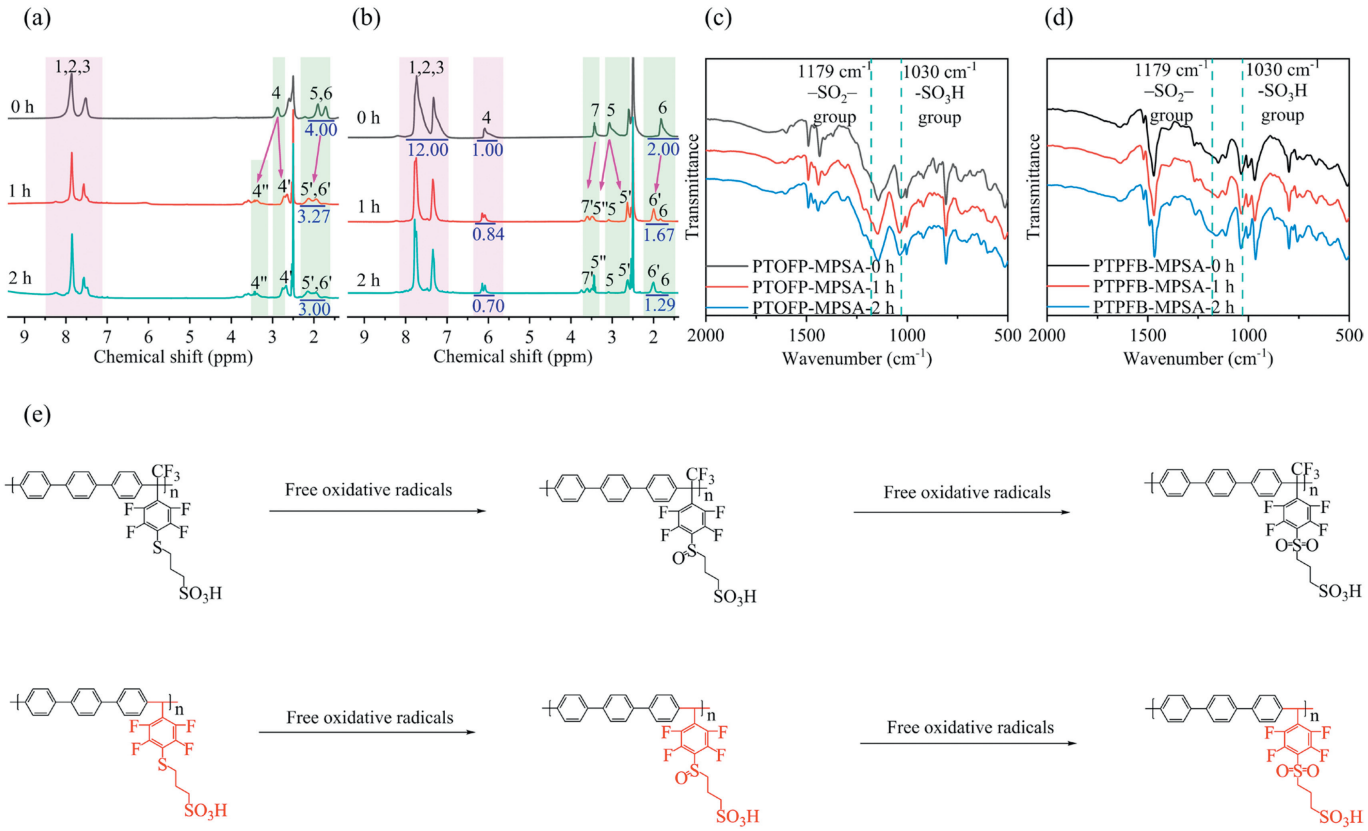

Fig. 3. ^{1}H NMR spectra of (a) PTOFP-MPSA and (b) PTPFB-MPSA, and FTIR spectra of (c) PTOFP-MPSA and (d) PTPFB-MPSA after the Fenton's treatment. (e) The possible mechanism diagram of -S- group as a free radical scavenger.

To assess the practical operation of PTOFP-MPSA and PTPFB-MPSA PEMs in the PEMFC, the MEAs were fabricated using a conventional catalyst-coated membrane technique. Initially, the Pt/C catalysts, water, isopropanol, and Nafion solution were ultrasonically mixed to produce the catalyst ink, sprayed homogeneously onto each side of the PEMs. After hot-pressing with two sheets of carbon paper, three MEAs prepared from PTOFP-MPSA, PTPFB-MPSA and Nafion 212 were subjected to a comparative analysis of their performance in H_2/air single cells under identical conditions (80 °C, 100% RH and 1 bar back pressure). The open-circuit voltage (OCV) of PTOFP-MPSA and PTPFB-MPSA was 0.946 V and 0.941 V, respectively, demonstrating that both membranes were well hermetically sealed. Fig. 4a illustrates that the peak power density of PTPFB-MPSA reaches 407 mW/cm^2, which is comparable to that of Nafion 212 (484 mW/cm^2). This phenomenon might be explained by the poor compatibility of PTPFB-MPSA with Nafion ionomers, which limits the increase in current density in the mass transport region. This effect is also reflected in the *I-V* plot of PTOFP-MPSA. In subsequent studies, we will develop alternative aromatic ionomers with improved compatibility to address this issue. Additionally, the peak power density of PTOFP-MPSA also reaches 312 mW/cm^2. Table S5 (Supporting information) presents a comparison of the fuel single-cell performance between the two membranes prepared in this work with the performance of recently published reports, indicating that the performance of the two membranes is comparable or even better than that of existing sulfonated hydrocarbon-based PEMs reported previously. The results indicates that PTOFP-MPSA and PTPFB-MPSA are promising for application in PEMFCs with high power density. As depicted in Fig. 4b, the OCV of PTPFB-MPSA with the highest peak power density

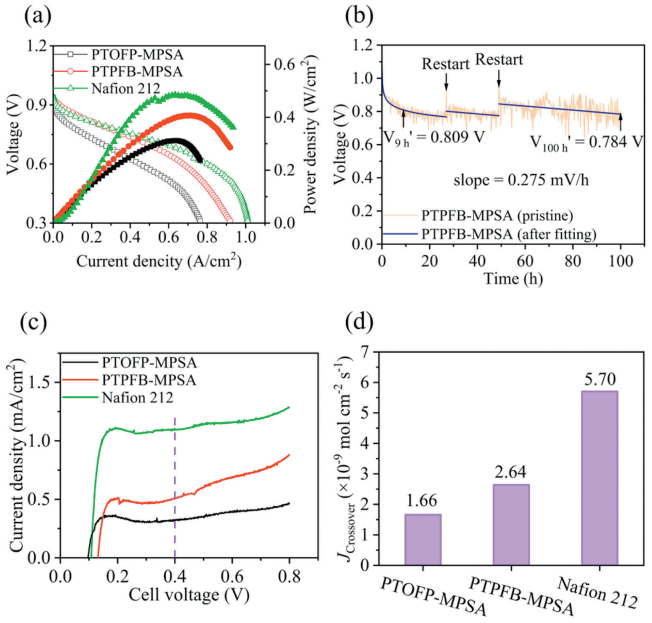

Fig. 4. (a) The fuel cell performance of PTOFP-MPSA, PTPFB-MPSA and Nafion 212 membranes at 80 °C. Test conditions: H_2 and air flow rates were 400 sccm, with 1 bar backpressure and 100% RH. (b) The OCV decay of PTPFB-MPSA membrane at 30% RH and 80 °C with H_2 and air flow rates of 400 sccm and 1 bar backpressure. (c) Hydrogen permeability curves of PTOFP-MPSA, PTPFB-MPSA and Nafion 212 membrane with 0.5 bar backpressure. (d) Hydrogen permeation flux ($J_{Crossover}$) through the membrane electrode of PTOFP-MPSA, PTPFB-MPSA and Nafion 212 membrane with 0.5 bar backpressure.

was evaluated over time under accelerated degradation conditions at 30% RH, while the remaining conditions were consistent with the performance tests. The cell underwent several restarts during the test because of gas replacement. Due to fluctuations in OCV resulting from the accelerated stress test conditions of low humidity (30% RH) and 1 bar backpressure, fitted curves were employed for the investigation of OCV decay [47]. The OCV value of PTPFB-MPSA decreased to 0.809 V in the first nine hours. This rapid decline can be attributed to the change in gas humidity on both sides, which is a nonlinear decline. Subsequently, the decay of the OCV becomes exceedingly gradual, ultimately reaching 0.784 V at the 100th hour with a decline rate of 0.275 mV/h. This result is superior to those in previous studies [32,48].

To verify the low hydrogen permeability of the two prepared membranes in fuel cells, the H_2 permeability of PTOFP-MSPA, PTPFB-MPSA, and Nafion 212 PEMs was evaluated by using LSV at 80 °C, 100% RH, and 0.5 bar backpressure. As detailed in Fig. 4c, the H_2 crossover current density of PTOFP-MPSA and PTPFB-MPSA was 0.32 and 0.51 mA/cm^2, respectively, considerably lower than that of Nafion 212 (1.10 mA/cm^2). This observation can be explained by the all-carbon aromatic backbone of PTOFP-MPSA and PTPFB-MPSA PEMs, which hinders the polymer segment movement and limits hydrogen crossover the membrane [18,49,50]. Notably, PTOFP-MPSA exhibited the lowest hydrogen permeation flux ($J_{Crossover}$) through the membrane electrode, which was only one-third of that of Nafion 212, as illustrated in Fig. 4d. This outcome can be explained by the additional -CF_3 group and higher molecular weight of PTOFP-MPSA, rendering the membrane with reduced hydrogen permeation current. In conclusion, both PTOFP-MPSA and PTPFB-MPSA demonstrate satisfactory single-cell performance and are thus suitable to be employed in fuel cell applications.

In summary, varieties of full-carbon fluorinated main chain polymers were prepared and grafted mercaptopropionic sulfonic acid pendant groups to produce novel PEMs using a superacid-catalyzed reaction and a subsequent *para*-fluoro-thiol click reaction. PEMs that had been prepared demonstrated excellent tensile strength and thermal stability, moderate proton conductivity, and low proton conduction activation energy. The synergistic effect of steady all-carbon fluorinated main chain and -S- linkage functioning as a scavenger of free radicals results in the superior antioxidant capacity of the prepared PEMs for application in PEMFCs. The Fenton's testing demonstrated that they also retained high residual weights. Furthermore, subsequent FT-IR and NMR spectroscopy validated the function of the grafted -S- linkage for scavenging free radicals. The PEMFC single cell based on PTPFB-MPSA displayed a power density of 407 mW/cm^2 under conditions of 1 bar back pressure and 80 °C when fed with 100% RH H_2/air. Moreover, the OCV decayed from 0.809 V at the end of the nonlinear decline to 0.784 V following 100 h running at 30% RH and 80 °C, displaying a decline rate of only 0.275 mV/h. Additionally, these membranes exhibited low hydrogen permeation current density, only 1/3 of Nafion 212 membrane. These findings reinforce the notion that the prepared PEMs show promising potential as the key components for PEMFCs.

Declaration of competing interest

The authors declare that they have no known competing financial interests or personal relationships that could have appeared to influence the work reported in this paper.

CRediT authorship contribution statement

Yuetong Gao: Writing – original draft, Investigation, Conceptualization. **Tong Mu:** Methodology, Investigation. **Xinyue Hu:** Data curation. **Yang Pang:** Methodology. **Chengji Zhao:** Writing – review & editing, Supervision, Resources.

Acknowledgment

This research was financially supported by the Development of Scientific and Technological Project of Jilin Province (No. 20230201139GX).

Supplementary materials

Supplementary material associated with this article can be found, in the online version, at doi:10.1016/j.cclet.2024.110763.

References

[1] I. Staffell, D. Scamman, A. Velazquez Abad, et al., Energy Environ. Sci. 12 (2019) 463–491.
[2] K. Espegren, S. Damman, P. Pisciella, I. Graabak, A. Tomasgard, Int. J. Hydrog. Energy 46 (2021) 23125–23138.
[3] M. Adamski, T.J.G. Skalski, B. Britton, et al., Angew. Chem. Int. Ed. 56 (2017) 9058–9061.
[4] H. Tang, K. Geng, L. Wu, et al., Nat. Energy 7 (2022) 153–162.
[5] I. Salmeron-Sanchez, P. Mansouri Bakvand, A. Shirole, et al., Chem. Eng. J. 474 (2023) 145879.
[6] E.H. Majlan, D. Rohendi, W.R.W. Daud, T. Husaini, M.A. Haque, Renew. Sust. Energ. Rev. 89 (2018) 117–134.
[7] Y. Wang, D.F. Ruiz Diaz, K.S. Chen, Z. Wang, X.C. Adroher, Mater. Today 32 (2020) 178–203.
[8] K. Jiao, J. Xuan, Q. Du, et al., Nature 595 (2021) 361–369.
[9] K. Oh, K. Ketpang, H. Kim, S. Shanmugam, J. Membr. Sci. 507 (2016) 135–142.
[10] M.D.T. Nguyen, S. Yang, D. Kim, J. Power Sources 328 (2016) 355–363.
[11] S. Yang, Y. Ahn, D. Kim, J. Mater. Chem. A 5 (2017) 2261–2270.
[12] C. Wang, H.Q. Li, Z. Wang, et al., Int. J. Hydrogen Energy 45 (2020) 29738–29748.
[13] V.D.C. Tinh, V.D. Thuc, D. Kim, J. Membr. Sci. 634 (2021) 119430.
[14] G. Wang, J. Li, H. Li, et al., Chin. Chem. Lett. 34 (2023) 107497.
[15] Z. Zhao, Q. Dai, S. Huang, et al., Chin. Chem. Lett. 35 (2024) 109231.
[16] X. Liu, Y. Zhang, S. Deng, et al., Chin. Chem. Lett. 30 (2019) 299–304.
[17] J. Li, N. Cui, D. Liu, et al., Int. J. Hydrogen Energy 50 (2024) 606–617.
[18] T. Li, S. Chai, B. Liu, C. Zhao, H. Li, J. Polym. Sci. 61 (2023) 2796–2814.
[19] N.R. Kang, T.H. Pham, P. Jannasch, ACS Macro Lett. 8 (2019) 1247–1251.
[20] H. Nederstedt, P. Jannasch, J. Membr. Sci. 647 (2022) 120270.
[21] P. Zuo, Y. Li, A. Wang, et al., Angew. Chem. Int. Ed. 59 (2020) 9564–9573.
[22] H. Lin, Y. Ma, X. Wang, et al., J. Membr. Sci. 695 (2024) 122479.
[23] T. Weissbach, T.J. Peckham, S. Holdcroft, J. Membr. Sci. 498 (2016) 94–104.
[24] Y. Park, D. Kim, J. Membr. Sci. 566 (2018) 1–7.
[25] M.J. Parnian, S. Rowshanzamir, A.K. Prasad, S.G. Advani, J. Membr. Sci. 556 (2018) 12–22.
[26] X. Liu, Y. Li, M. Li, et al., J. Membr. Sci. 629 (2021) 119282.
[27] P. Wang, C. Cai, J. Tan, M. Pan, Int. J. Hydrogen Energy 46 (2021) 34867–34873.
[28] L. Zhou, J. Zhu, M. Lin, et al., J. Energy Chem. 40 (2020) 57–64.
[29] J. Wang, Y. Dai, R. Wan, et al., Chem. Eng. J. 413 (2021) 127541.
[30] G. Delaittre, L. Barner, Polym. Chem. 9 (2018) 2679–2684.
[31] S. Cai, C. Wang, Z. Tao, et al., Int. J. Hydrogen Energy 47 (2022) 9319–9330.
[32] B. Xue, M.Z. Zhu, S.Q. Fu, et al., J. Membr. Sci. 673 (2023) 121263.
[33] L.H. Sperling, Introduction to Physical Polymer Science, 4th ed., John Wiley & Sons Inc., 2005, pp. 349–425.
[34] N. Chen, H.H. Wang, S.P. Kim, et al., Nat. Commun. 12 (2021) 2367.
[35] F. Xu, Y. Chen, J. Li, et al., J. Membr. Sci. 664 (2022) 121045.
[36] D. Qiu, L. Peng, X. Lai, M. Ni, W. Lehnert, Renew. Sust. Energ. Rev. 113 (2019) 109289.
[37] M. Mohammadi, S. Mehdipour-Ataei, Renew. Energ. 158 (2020) 421–430.
[38] M. Pan, C. Pan, C. Li, J. Zhao, Renew. Sust. Energ. Rev. 141 (2021) 110771.
[39] L. Liu, Y. Wang, S. Liu, et al., J. Membr. Sci. 660 (2022) 120774.
[40] Y. Zhu, L. Ding, X. Liang, et al., Energy Environ. Sci. 11 (2018) 3472–3479.
[41] S. Zhang, X. Li, Y. Yang, et al., J. Membr. Sci. 698 (2024) 122587.
[42] S. Mu, C. Xu, Q. Yuan, et al., J. Appl. Polym. Sci. 129 (2013) 1586–1592.
[43] H. Hou, M.L. Di Vona, P. Knauth, ChemSusChem 4 (2011) 1526–1536.
[44] T. Ban, M. Guo, Y. Wang, Y. Zhang, X. Zhu, J. Membr. Sci. 668 (2023) 121255.
[45] D. Zhao, J. Li, M.K. Song, et al., Adv. Energy Mater. 1 (2011) 203–211.
[46] C. He, K.F. Han, J.H. Yu, H. Zhu, Z.M. Wang, Eur. Polym. J. 74 (2016) 168–179.
[47] V.D.C. Tinh, V.D. Thuc, Y. Jeon, G.Y. Gu, D. Kim, J. Membr. Sci. 660 (2022) 120903.
[48] A.M. Baker, L. Wang, W.B. Johnson, A.K. Prasad, S.G. Advani, J. Phys. Chem. C 118 (2014) 26796–26802.
[49] W. Li, R. Zhang, X. Zhao, et al., J. Mater. Chem. A 11 (2023) 4547–4558.
[50] T. Vu Dong, V.D.C. Tinh, D. Kim, J. Power Sources 556 (2023) 232418.